ELSEVIER

Journal of Chromatography A, 911 (2001) 167–175

JOURNAL OF CHROMATOGRAPHY A

www.elsevier.com/locate/chroma

Approximation function for the direct calculation of rate constants and Gibbs activation energies of enantiomerization of racemic mixtures from chromatographic parameters in dynamic chromatography

Oliver Trapp*, Volker Schurig

Institute of Organic Chemistry, University of Tübingen, Auf der Morgenstelle 18, D-72076 Tübingen, Germany

Received 29 August 2000; received in revised form 5 December 2000; accepted 13 December 2000

Abstract

An approximation function for enantioselective dynamic chromatography of racemic mixtures of interconverting enantiomers has been derived that allows the direct calculation of enantiomerization rate constants (k_1 and k_{-1}) and Gibbs activation energies of enantiomerization, $\Delta G^{\neq}$, from chromatographic parameters, i.e., retention times of the enantiomers A and B (t_R^A and t_R^B), peak widths at half height (w_A and w_B) and the relative plateau height ($h_{plateau}$), without computer simulation. The reaction rate constants of enantiomerization, k_{-1}, obtained with this approximation function, have been validated by comparison with a simulated dataset of 15 625 chromatograms. The mean, standard deviation and confidence interval show a high correlation between the approximated and simulated rate constants. The average deviation from the Gibbs activation enthalpy of enantiomerization, $\Delta G^{\neq}$, has been estimated to be as small as about ± 0.11 *RT*.

Keywords: Enantiomerization kinetics; Dynamic chromatography; Computer simulations; Rate constants; Stochastic model; Theoretical plate model; Inversion barrier; Enantiomerization barrier

1. Introduction

In recent years, dynamic chromatography has increasingly been employed for the determination of rate constants of reactions proceeding during the time scale of partitioning, particularly the reversible interconversion of stereoisomers, i.e., enantiomerization, epimerization and diastereomerization. Enantioselective dynamic chromatography has previously been applied to the determination of enantiomerization barriers [1–21] and the interconversion rate of the spin isomers o-H_2 and p-H_2 [22,23].

Enantiomerization constitutes a reversible first-order reaction [1,24], which arises from the interconversion of a stereogenic element in a particular molecule. In enantioselective chromatography, typical peak profiles, such as peak broadening, plateau formation and, eventually, peak coalescence, can be observed, and are occasionally even considered as a complication of the separation process. Yet, in enantioselective dynamic chromatography, the characteristic peak profiles not only represent a diagnostic

*Corresponding author. Tel.: +49-7071-29-76257; fax: +49-7071-29-5538.

E-mail address: o1iver.trapp@uni-tuebingen.de (O. Trapp).

0021-9673/01/$ – see front matter
PII: S0021-9673(00)01259-0

tool for an interconversion process itself but are a prerequisite for the determination of enantiomerization barriers [1]. Depending on the enantiomerization barrier, different dynamic chromatographic or electrophoretic techniques (e.g. DGC, DSFC, DHPLC, DCE, DCEC, DMEKC) may be selected for the quantification of the enantiomerization process at a given time scale of separation and temperature.

The rate constant and the kinetic activation parameters of enantiomerization are obtained by iterative comparison of experimental and simulated chromatograms. The first simulation program based on the theoretical plate model [25–28] was published in 1984 [1] and was later extended to simulations of up to 120 000 effective plates (SIMUL) [5,29]. The theoretical plate model illustrates the chromatographic separation as a discontinuous process, assuming that all steps proceed repeatedly in separate uniform sections of a multi-compartmentalized column, with N theoretical plates considered as chemical reactors. Three basic steps are performed in every plate: (1) distribution of the enantiomers A and B, (2) the enantiomerization process and (3) shifting of the mobile phase to the next plate (cf. Scheme 1).

The application of the principle of microscopic reversibility [1] requires that the rates of interconversion of the two enantiomers are rendered different in the presence of the chiral stationary phase (CSP). This notion is due to the fact that the enantiomers are discriminated, and hence separated, due to a different thermodynamic Gibbs free energy ($\Delta_{A,B}$, $\Delta G = RT \ln(K_B/K_A)$), as shown in Scheme 1.

The equilibrium constant, K^{CSP}, in the chiral stationary phase depends on the two phase-distribution constants (=partition coefficients), K_A and K_B, according to the principle of microscopic reversibility [1,5,18]:

$$K^{CSP} = \frac{K_B}{K_A} = \frac{k'_B}{k'_A} = \frac{k_1^{CSP}}{k_{-1}^{CSP}} \frac{k_{-1}^{mob}}{k_1^{mob}} \quad (1)$$

Thus, whereas the second eluted enantiomer is enriched during the chromatographic timescale because it is formed more rapidly than the first eluted enantiomer ($k_1^{CSP} > k_{-1}^{CSP}$), no overall deracemization, occurs as the second eluted enantiomer is depleted to a greater extent due to its longer residence time in the column.

This implies that the backward reaction rate constant, k_{-1}^{CSP}, is already determined for given values of k_1^{CSP} and the retention factors k'_A and k'_B, calculated from the total retention time, t_R, and the mobile-phase hold-up time, t_M, according to $k' = (t_R - t_M)/t_M$:

$$k_{-1}^{CSP} = \frac{k'_A}{k'_B} k_1^{CSP} \quad (2)$$

However, from computer simulation of elution profiles of a dynamic chromatographic experiment, it is not possible to differentiate between the rate constants in the mobile phase and the chiral stationary phase (CSP). Only apparent rate constants (k_1^{app} and k_{-1}^{app}), which are means of the forward and backward rate constants of the mobile and chiral stationary phase, weighted by the retention factors k'_A and k'_B, can be determined. Taking into account that the backward reaction rate can be calculated from the forward reaction rates, the following equations can be derived [5,18,20]:

$$k_1^{app} = \frac{1}{1+k'_A} k_1^{mob} + \frac{k'_A}{1+k'_A} k_1^{CSP}$$
$$k_{-1}^{app} = \frac{1}{1+k'_B} k_1^{mob} + \frac{k'_B}{1+k'_B} k_{-1}^{CSP} \quad (3)$$

In cases where the rate constants in the mobile gas and stationary liquid phase are equal ($k_1^{mob} = k_1^{CSP}$; $k_{-1}^{mob} = k_{-1}^{CSP}$), the apparent rate constants (k_1^{app} and k_{-1}^{app}) are given by:

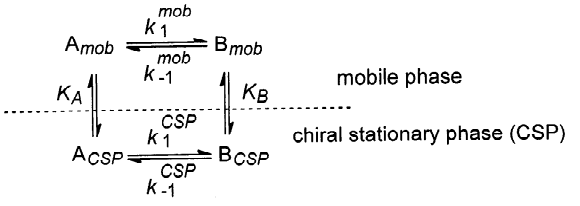

Scheme 1. Equilibrium in a theoretical plate: A is the first eluted enantiomer, B is the second eluted enantiomer, k_1 and k_{-1} represent the forward and backward reaction rate constants in the mobile phase (mob) and chiral stationary phase (CSP), respectively, and K denotes the distribution constant.

$$k_1^{app} = k_1^{mob} = k_1^{CSP}$$
$$k_{-1}^{app} = k_{-1}^{mob} = k_{-1}^{CSP} \quad (4)$$

Supposing this assumption is fulfilled, the rate constants of enantiomerization in the chiral stationary phase and mobile phase are directly obtained by dynamic chromatography. However, Eq. (4) is not a prerequisite to determine rate constants by dynamic chromatography, since the apparent rate constants are in a fixed ratio of the rate constants of enantiomerization in the chiral stationary phase and mobile phase for given chromatographic parameters (Eq. (3)).

If the rate constants in the gas phase are accessible by an independent method, it is possible to calculate the rate constants in the stationary liquid phase and to determine catalytic or inhibitive effects of the chiral stationary phase, as previously described [18,21].

The stochastic model, based on the simulation of Gaussian distribution functions, $\Phi_i(t')$ [with i=(A and B) and the running time t'] and using a time-dependent probability density function, $\Psi(t')$, for the interconverting enantiomers, has also been applied for the determination of enantiomerization barriers [2–4,23,30,31]. Both models have been combined in the computer program ChromWin [18,20], which allows a fast and efficient simulation and evaluation of experimental chromatograms without restrictions referring to plate numbers, N.

Another approach for the determination of enantiomerization rate constants from dynamic chromatographic experiments is the continuous flow model, which utilizes equations derived from chemical engineering for the chromatographic system [32–35].

In contrast to these ab-initio-type simulations, semiempirical peak deconvolution methods have also been developed to estimate rate constants of enantiomerization and isomerization, k_1 [36–43]. The ratios of the interconverted and non-interconverted analytes can be obtained by graphical integration of the peak areas [36].

Since the simulation of experimental chromatograms is computationally expensive, Kramer [31] attempted to derive an equation, based on the stochastic model, to calculate the reaction rate constants, k_1, from chromatographic parameters. However, the reaction rate constant, k_1, could not be isolated from the Γ-function, an approximated solution of Giddings probability distribution, and, therefore, recursive simulation was again necessary to refine the value of the reaction rate constant, k_1.

In the present study, we derived an approximation function, based on the stochastic model, which allows for the first time the calculation of rate constants of enantiomerization, k_1, of a racemic mixture directly from the chromatographic parameters, i.e., retention times of the enantiomers A and B (t_R^A and t_R^B), peak widths at half height (w_A and w_B) and the relative plateau height ($h_{plateau}$), without computer simulation. This approximation function has been validated by comparison to a dataset of 15 625 chromatograms with conditions commonly encountered in dynamic chromatography.

2. Experimental

To validate the approximation function, a dataset of 15 626 chromatograms was simulated with the recently developed computer program ChromWin (release 4.0), which is compatible both with the discontinuous plate model and the stochastic model, and runs under Windows 95/98/NT/2000 on an IBM-compatible personal computer. For the calculation, the stochastic model was employed with the following window of parameters: hold-up time, t_M = 0.5 . . . 2.5 min; retention time of first-eluted enantiomer, t_R^A = 8.0 . . . 40.0 min; separation factor, α = 1.05 . . . 2.00; mean number of theoretical plates, N = 20 000 . . . 200 000; threshold, 10^{-15} mol; rate constant of enantiomerization in the mobile phase, $k_1^{mob} = 1.0 \cdot 10^{-5} \ldots 1.0 \cdot 10^{-3}$ s^{-1} and rate constant of enantiomerization in the chiral stationary phase $k_1^{CSP} = 1.0 \cdot 10^{-5} \ldots 1.0 \cdot 10^{-3}$ s^{-1}. Each of these parameter ranges was divided into five equidistant steps. The calculation was finished within four days on a personal computer with an Intel Pentium III 600 MHz processor. With the dataset evaluation method of ChromWin, approximated rate constants k_1^{approx} were determined from the chromatographic parameters of 15 461 chromatograms. Since the width at half height, w_h, of 165 chromatograms could not be

evaluated by the standard integration method, due to strong overlapping of the peaks, these chromatograms were neglected in the statistical analysis.

3. Results and discussion

As mentioned above, the elution profile, $P(t')$[1] (cf. Eq. (5)), with the running time, t', for interconverting enantiomers during the separation process is given by the sum of the two distribution functions $\Phi_A(t')$ and $\Phi_B(t')$ of the non-interconverted enantiomers, and the probability density functions, $\Psi_A(t')$ and $\Psi_B(t')$ of the interconverted enantiomers:

$$P(t') = \Phi_A(t') + \Phi_B(t') + \Psi_A(t') + \Psi_B(t') \quad (5)$$

Since the time-dependent concentration profile, $\bar{c}(t')$, of the interconverting enantiomers has to be Gaussian-modulated and the integral cannot be solved analytically, the probability density functions, $\Psi_A(t')$ and $\Psi_B(t')$, have to be calculated numerically.

Therefore, the strategy was (i) to calculate distribution functions, $\Phi_A(t')$ and $\Phi_B(t')$, of the non-interconverted enantiomers, (ii) to replace the time-dependent profile, $\bar{c}(t')$, by a function for which the concentration is time-independent and the integral of the Gaussian modulation can be approximated. From these functions, the concentration at the peak retention times, t_R^A and t_R^B, and the concentration at the plateau in the time-middle, $\bar{t}(\bar{t} = (t_R^A + t_R^B)/2)$ can be calculated, which allows one to correlate the relative plateau height, $h_{plateau}$, with the reaction rate of the enantiomerization (cf. Fig. 1).

The concentration–time area of the non-interconverted enantiomers, c_i', is calculated from first-order kinetics with the reaction rate, k, reaction time, t, and the initial concentration–time area, c^0, according to Eq. (6):

$$c_i' = c_i^0 e^{-kt} \quad \text{with } i = \{A,B\} \quad (6)$$

To evaluate the remaining concentration–time area of enantiomer A, the apparent forward reaction rate,

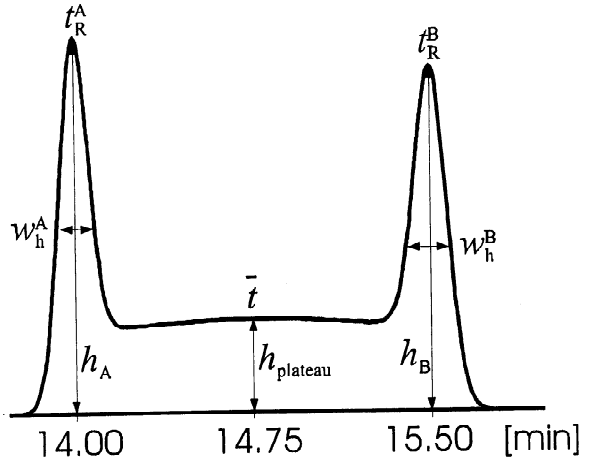

Fig. 1. Example of an elution profile of interconverting enantiomers with the experimental parameters needed for calculation. Simulation parameters: stochastic model, $t_M = 1.0$ min, $t_R^A = 14.0$ min, $t_R^B = 15.5$ min, $N = 50\ 000$ and $k_1^{app} = 1 \cdot 10^{-3}$ s^{-1}. Parameters calculated from the chromatogram: widths at half height, $w_A = 9.42$ s, $w_B = 10.72$ s and $h_{plateau} = 24.81\%$.

k_1^{app}, and the retention time, t_R^A, and for enantiomer B, the apparent backward reaction rate, k_{-1}^{app}, and the retention time, t_R^B, are applied to Eq. (6). These two different reaction rates and reaction times complicate the derivation of a function of k_1. Therefore, the following approximation has to be used, considering that the concentration–time area of the enantiomers after the chromatographic separation process is equal due to the principle of microscopic reversibility [1]:

$$k_1^{approx} t_R^A = k_1^{app} t_R^A \approx k_{-1}^{approx} t_R^B \quad (7)$$

With the approximated forward reaction rate, k_1^{approx}, and the total retention time, t_R^A, of enantiomer A, the distribution functions $\Phi_A(t')$ and $\Phi_B(t')$ of the non-interconverted enantiomers A and B can be calculated according to Eqs. (8a) and (8b):

$$\Phi_i(t') = \frac{c_i'}{\sigma_i \sqrt{2\pi}} e^{-\frac{(t' - t_R')^2}{2\sigma_i^2}} \quad \text{and}$$

$$\sigma_i = \frac{w_i}{\sqrt{8 \ln 2}} \quad \text{with } i = \{A,B\} \quad (8a,b)$$

The concentration–time area of the plateau $c_{plateau}$ is obtained from the mass balance ($c_A^0 + c_B^0 = c_A' + c_B' + c_{plateau}$), considering that the concentration–time area, c, is proportional to the amount, n. The

[1] The concentration–time areas c^0, c' and $c_{plateau}$ [mol·s l^{-1}] are proportional to the amount of analyte, and the functions $\Psi(t')$, $\Phi(t')$, $P(t')$, $\bar{c}(t')$ and $\bar{c}_{boxcar}(t')$ [mol l^{-1}] give the concentration at the running time, t', of the elution profile.

division of the plateau concentration, c_{plateau}, by the difference of the retention time of the two enantiomers ($t_R^B - t_R^A$) gives the concentration at the running time, t', of a boxcar-function, $\bar{c}_{\text{boxcar}}(t')$ (cf. Eq. (9)), which approximates the probability density function of ideal and linear chromatography derived by Keller and Giddings [30]. The approximated concentration function $\bar{c}_{\text{boxcar}}(t')$ describes the profile only for a racemic mixture of the enantiomers A and B. For mixtures deviating from a 1:1 ratio of the enantiomers, a gradient has to be introduced:

$$\bar{c}_{\text{boxcar}}(t_R^A <= t' <= t_R^B) = \frac{c_{\text{plateau}}}{t_R^B - t_R^A} = \frac{c_A^0 - c'_A + c_B^0 - c'_B}{t_R^B - t_R^A} \quad (9)$$

To estimate the deviation of the derived boxcar-function from the curvature of the probability density function of ideal chromatography, several scenarios were simulated. In Fig. 2, the mean deviation of the boxcar-function from the probability function of ideal chromatography as a function of the rate constant is shown. With an increasing rate constant, the mean deviation increased by up to 4%.

The next step is the Gaussian modulation of the concentration function, $\bar{c}_{\text{boxcar}}(t')$, with the integration variable, t, and the running time, t' (cf. Eq. (10)), to obtain the concentration profile, $\Psi(t')$, of non-ideal linear chromatography. Since the boxcar-function consists of a time-independent constant, it can be factored out of the integral:

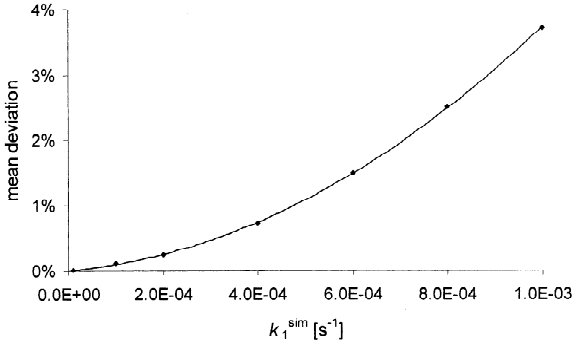

Fig. 2. Mean deviation of the boxcar-function from the probability density function of ideal chromatography as a function of the rate constant. Simulation parameters: stochastic model, $t_M = 1.0$ min, $t_R^A = 14.0$ min, $t_R^B = 15.5$ min and $N = 50\ 000$.

$$\Psi(t') = \frac{\bar{c}_{\text{boxcar}}(t')}{\sqrt{\pi}} \int_{t_1}^{t_2} \sqrt{\frac{N}{2}}\, e^{-\frac{N}{2}\left(\frac{t-t'}{t}\right)^2} \frac{1}{t}\, dt \quad (10)$$

To simplify the integral of Eq. (10), a substitution with Eq. (11a) is applied and the integration variable dt is transformed to dv according to Eqs. (11b) and (11c):

$$v = \sqrt{\frac{N}{2}}\frac{t-t'}{t} \qquad \frac{dv}{dt} = \sqrt{\frac{N}{2}}\frac{t'}{t^2}$$

$$t = \frac{t'}{1 - \sqrt{\frac{2}{N}}\, v} \quad (11a,b,c)$$

The boundaries are also transformed with Eq. (11a) considering that $\bar{c}_{\text{boxcar}}(t')$ is zero for $t' < t_R^A$ and $t' > t_R^B$ (Table 1).

The resulting integral cannot be solved analytically, but the numerical integration gives a limit for Eq. (12) with high plate numbers, N:

$$\Psi(v) = \frac{\bar{c}_{\text{boxcar}}(t')}{\sqrt{\pi}} \int_{v_1}^{v_2} \frac{e^{-v^2}}{1 - \sqrt{\frac{2}{N}}\, v}\, dv = \frac{\bar{c}_{\text{boxcar}}(t')}{\sqrt{\pi}} \lim_{N\to\infty} \int_{v_1}^{v_2} \frac{e^{-v^2}}{1 - \sqrt{\frac{2}{N}}\, v}\, dv \quad (12)$$

In Table 2, the results of the numerical integration are summarized.

The integral converges at the retention times t_R^A and t_R^B to a value of 0.5. The solution of the integral can be corrected for lower plate numbers by empirical adding $1/\sqrt{2\pi N}$ to 0.5 at the retention time t_R^A (boundaries of the integral 0 and $+\infty$) and empirical subtracting $1/\sqrt{2\pi N}$ from 0.5 for t_R^B (boundaries of the integral $-\infty$ and 0). At the time-middle, $\bar{t}$($\bar{t} = t_R^A + t_R^B)/2$), the solution of the integral is about 1.0.

Table 1
Transformation of the lower and upper limit of the integral

	t_1	t_2	v_1	v_2
$\Psi(t_R^A)$	t_R^A	t_R^B	0	$\to\infty$
$\Psi(t_R^B)$	t_R^A	t_R^B	$\to -\infty$	0
$\Psi(\bar{t})$	t_R^A	t_R^B	$\to -\infty$	$\to\infty$

Table 2
Results of the integral (11) as a function of the plate number, N

N	$\int_0^\infty \frac{e^{-v^2}}{1-\sqrt{\frac{2}{N}}\,v}\,dv$	$\int_{-\infty}^0 \frac{e^{-v^2}}{1-\sqrt{\frac{2}{N}}\,v}\,dv$	$\int_{-\infty}^\infty \frac{e^{-v^2}}{1-\sqrt{\frac{2}{N}}\,v}\,dv$
10	0.872	0.407	1.280
100	0.546	0.464	1.010
1000	0.513	0.488	1.001
2000	0.509	0.491	1.001
5000	0.505	0.494	1.000
10 000	0.504	0.496	1.000
50 000	0.502	0.498	1.000
100 000	0.501	0.498	1.000
1 000 000	0.500	0.499	1.000
10 000 000	0.500	0.500	1.000

Eqs. (13a,b,c) represent the solution of the concentration profile at times t_R^A, t_R^B and $\bar{t}$:

$$\Psi(t_R^A) \approx \left(0.5 + \frac{1}{\sqrt{2\pi N}}\right)\bar{c}_{boxcar}(t_R^A)$$

$$\Psi(t_R^B) \approx \left(0.5 - \frac{1}{\sqrt{2\pi N}}\right)\bar{c}_{boxcar}(t_R^B)$$

$$\Psi(\bar{t}) \approx 1.0\bar{c}_{boxcar}(\bar{t}) \qquad (13a,b,c)$$

Combining the contributions of the distribution functions $\Phi_A(t')$, $\Phi_B(t')$ and the concentration profile $\Psi(t')$ allows the calculation of the concentrations, $c(t')$, at the retention times t_R^A, t_R^B and $\bar{t}$ of the interconversion profile. This is a prerequisite in order to be able to correlate the relative peak heights, h_A and h_B, with the relative plateau height, $h_{plateau}$ (cf. Eqs. (14), (15) and (16)):

$$c(t_R^A) = \Phi_A(t_R^A) + \Psi(t_R^A) + \Phi_B(t_R^A)$$
$$= \left(0.5 - \frac{1}{\sqrt{2\pi N}}\right)\frac{c_A^0 + c_B^0}{(t_R^B - t_R^A)}\left(1 - e^{-k_1^{approx} t_R^A}\right)$$
$$+ \frac{c_A^0}{\sigma_A\sqrt{2\pi}}\, e^{-k_1^{approx} t_R^A}$$
$$+ \frac{c_B^0}{\sigma_B\sqrt{2\pi}}\, e^{-k_1^{approx} t_R^A} e^{-\frac{(t_R^A - t_R^B)^2}{2\sigma_B^2}} \qquad (14)$$

$$c(t_R^B) = \Phi_A(t_R^B) + \Psi(t_R^B) + \Phi_B(t_R^B)$$
$$= \left(0.5 - \frac{1}{\sqrt{2\pi N}}\right)\frac{c_A^0 + c_B^0}{(t_R^B - t_R^A)}\left(1 - e^{-k_1^{approx} t_R^A}\right)$$
$$+ \frac{c_A^0}{\sigma_A\sqrt{2\pi}}\, e^{-k_1^{approx} t_R^A} e^{-\frac{(t_R^B - t_R^A)^2}{2\sigma_A^2}}$$
$$+ \frac{c_B^0}{\sigma_B\sqrt{2\pi}}\, e^{-k_1^{approx} t_R^A} \qquad (15)$$

$$c(\bar{t}) = \Phi_A(\bar{t}) + \Psi(\bar{t}) + \Phi_B(\bar{t})$$
$$= \frac{c_A^0 + c_B^0}{t_R^B - t_R^A}\left(1 - e^{-k_1^{approx} t_R^A}\right)$$
$$+ \frac{c_A^0}{\sigma_A\sqrt{2\pi}}\, e^{-k_1^{approx} t_R^A} e^{-\frac{(t_R^B - t_R^A)^2}{8\sigma_A^2}}$$
$$+ \frac{c_B^0}{\sigma_B\sqrt{2\pi}}\, e^{-k_1^{approx} t_R^A} e^{-\frac{(t_R^A - t_R^B)^2}{8\sigma_B^2}} \qquad (16)$$

The relative plateau height, $h_{plateau}$, is defined as the ratio of the concentration at the time-middle, $\bar{t}$, and the concentration of the higher peak at the retention times t_R^A and t_R^B of enantiomer A or B.

Therefore, two cases (i) and (ii) have to be differentiated:

(i) $c(t_R^A)$ is higher than $c(t_R^B)$ and $h_{plateau}$ is defined by Eq. (17):

$$h_{\text{plateau}} = 100\,\frac{c(\bar{t})}{c(t_{\text{R}}^{\text{A}})} \tag{17}$$

Substitution of this expression with Eqs. (14) and (16) gives the final approximation function for k_1^{approx}:

$$k_1^{\text{approx}} =$$
$$-\frac{1}{t_{\text{R}}^{\text{A}}}\ln\left[\frac{(c_{\text{A}}^0+c_{\text{B}}^0)}{(t_{\text{R}}^{\text{B}}-t_{\text{R}}^{\text{A}})}\left(1-\frac{h_{\text{plateau}}}{100}\left(0.5+\frac{1}{\sqrt{2\pi N}}\right)\right)\right]$$
$$-\frac{1}{t_{\text{R}}^{\text{A}}}\ln\left[\frac{(c_{\text{A}}^0+c_{\text{B}}^0)}{(t_{\text{R}}^{\text{B}}-t_{\text{R}}^{\text{A}})}\left(1-\frac{h_{\text{plateau}}}{100}\left(0.5+\frac{1}{\sqrt{2\pi N}}\right)\right)\right.$$
$$+c_{\text{A}}^0\,\frac{0.01h_{\text{plateau}}-\mathrm{e}^{-\frac{(t_{\text{R}}^{\text{B}}-t_{\text{R}}^{\text{A}})^2}{8\sigma_A^2}}}{\sigma_{\text{A}}\sqrt{2\pi}}$$
$$\left.+c_{\text{B}}^0\,\frac{0.01h_{\text{plateau}}\,\mathrm{e}^{-\frac{(t_{\text{R}}^{\text{A}}-t_{\text{R}}^{\text{B}})^2}{2\sigma_{\text{B}}^2}}-\mathrm{e}^{-\frac{(t_{\text{R}}^{\text{A}}-t_{\text{R}}^{\text{B}})^2}{8\sigma_{\text{B}}^2}}}{\sigma_{\text{B}}\sqrt{2\pi}}\right] \tag{18}$$

(ii) Eqs. (19) and (20) can be evaluated correspondingly:

$$h_{\text{plateau}} = 100\,\frac{c(\bar{t})}{c(t_{\text{R}}^{\text{B}})} \tag{19}$$

$$k_1^{\text{approx}} =$$
$$-\frac{1}{t_{\text{R}}^{\text{A}}}\ln\left[\frac{(c_{\text{A}}^0+c_{\text{B}}^0)}{(t_{\text{R}}^{\text{B}}-t_{\text{R}}^{\text{A}})}\left(1-\frac{h_{\text{plateau}}}{100}\left(0.5-\frac{1}{\sqrt{2\pi N}}\right)\right)\right]$$
$$-\frac{1}{t_{\text{R}}^{\text{A}}}\ln\left[\frac{(c_{\text{A}}^0+c_{\text{B}}^0)}{(t_{\text{R}}^{\text{B}}-t_{\text{R}}^{\text{A}})}\left(1-\frac{h_{\text{plateau}}}{100}\left(0.5-\frac{1}{\sqrt{2\pi N}}\right)\right)\right.$$
$$+c_{\text{A}}^0\,\frac{0.01h_{\text{plateau}}\,\mathrm{e}^{-\frac{(t_{\text{R}}^{\text{B}}-t_{\text{R}}^{\text{A}})^2}{2\sigma_{\text{A}}^2}}-\mathrm{e}^{-\frac{(t_{\text{R}}^{\text{B}}-t_{\text{R}}^{\text{A}})^2}{8\sigma_{\text{A}}^2}}}{\sigma_{\text{A}}\sqrt{2\pi}}$$
$$\left.+c_{\text{B}}^0\,\frac{0.01h_{\text{plateau}}-\mathrm{e}^{-\frac{(t_{\text{R}}^{\text{A}}-t_{\text{R}}^{\text{B}})^2}{8\sigma_{\text{B}}^2}}}{\sigma_{\text{B}}\sqrt{2\pi}}\right] \tag{20}$$

The approximated backward reaction rate constant of enantiomerization k_{-1}^{approx} can be calculated from the forward reaction rate constant using Eq. (7).

Applying Eq. (18) to the chromatogram depicted in Fig. 1, the solution is $k_1^{\text{approx}} = 9.766 \cdot 10^{-4}\ \text{s}^{-1}$. This is in good accordance with the input value $k_1^{\text{app}} = 1.0 \cdot 10^{-3}\ \text{s}^{-1}$ (relative error, 2.34%). Values from the standard integration procedure of ChromWin [18,20], implemented in common integrators and data acquisition software systems, has been used as input parameters, since the theoretical values of an experiment are usually unknown.

4. Validation

Deviations of the approximated rate constant arise from the aberration of the boxcar-function from the probability density function of ideal chromatography and the additional broadening of the peaks caused by enantiomerization.

To validate the approximation functions of k_1^{approx} [Eqs. (18) and (20)], and to estimate the error, a dataset of 15 625 chromatograms has been simulated with ChromWin [18,20], as described in detail in the Experimental section. A total of 165 chromatograms were excluded from the evaluation procedure, because strong overlapping of the peaks made a determination of the width at half height impossible.

Using the chromatographic parameters, which were also determined by the standard integration method of ChromWin [18,20], the dataset was evaluated with the approximation function, Eqs. (18) and (20), and the values obtained from this were compared with the apparent rate constants, k_1^{app}, of the input parameters.

In Table 3, selected values of the statistical analysis are summarized. Fig. 3 gives a plot of k_1^{app} vs. k_1^{approx}, showing the high correlation between the approximated and simulated rate constants. Linear

Table 3
Selected values of the statistical analysis of the dataset obtained by ChromWin [18,20] on the basis of the stochastic model

k_1^{sim} [10^{-5} s^{-1}]	k_1^{approx} [10^{-5} s^{-1}]	σ_{approx} [10^{-5} s^{-1}]	n
1.0	0.99±0.01*	0.01	625
25.8	26.13±0.06	0.43	650
50.5	51.26±0.23	1.71	623
75.3	78.33±0.62	4.77	650
100.0	105.50±0.82	6.11	601

* Deviation calculated using a confidence interval of 99.9%.

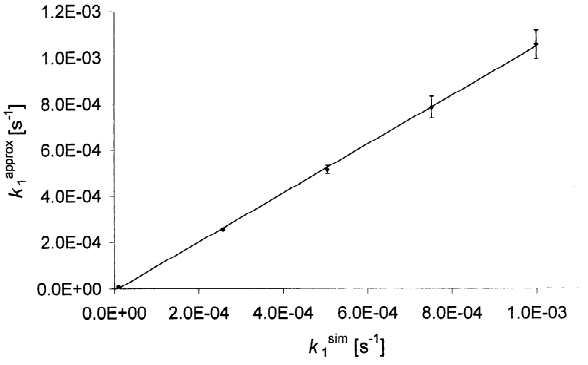

Fig. 3. Comparison of reaction rates from simulation, k_1^{app}, and from the approximation function, k_1^{approx}. The error bars represent the standard deviation, σ, of k_1^{approx}.

regression gives $k_1^{approx} = 1.056 \times k_1^{app} - 1 \cdot 10^{-5}$ (correlation coefficient $r = 0.999$; standard error $S = 3.2727 \cdot 10^{-5}$).

To estimate the maximum error within the standard deviation, σ, of the approximated reaction rate, k_1^{approx}, from the simulated reaction rate, k_1^{app}, the approximated reaction rate, k_1^{approx}, is multiplied by the correlation factor of the slope (1.056) and the relative standard deviation (RSD) for $k_1^{app} = 1 \cdot 10^{-3}$ s^{-3} (5.8%). This gives an error of $\pm 11.7\%$ for the approximated rate constant, k_1^{approx}. The deviation of the Gibbs activation energy is $\Delta G^{\neq} = -RT \ln(\pm 11.7\%) = \pm 0.11RT$.

At a temperature $T = 375$ K the deviation of $\Delta G^{\neq}$ amounts to 0.34 kJ mol^{-1} compared to the value obtained by computer simulation.

5. Conclusions

The function derived here for the calculation of interconversion rate constants in enantioselective dynamic chromatography constitutes a valuable tool for every analytical chemist who has to deal with stereolabile molecules. It allows, in the simplest procedure available to date, the calculation of rate constants directly from the experimental parameters with acceptable accuracy, as proven by the comparison of the approximated values with those obtained from the simulation. For higher demands, as are commonly encountered, e.g. in the pharmaceutical industry or required by regulatory authorities, the derived equation can give a first hint, if the exact calculation with a simulation program such as ChromWin is indicated. In this case, the value calculated by the derived equations provides a good starting value for the simulation of chromatograms and thereby reduces the number of refinement steps and accelerates the calculation process.

Acknowledgements

This work was supported by Deutsche Forschungsgemeinschaft, Fonds der chemischen Industrie and the Graduiertenkolleg ‘Chemistry in Interphases’. OT thanks the Stiftung Stipendien-Fonds der chemischen Industrie for a doctorate scholarship.

References

[1] W. Bürkle, H. Karfunkel, V. Schurig, J. Chromatogr. 288 (1984) 1.
[2] A. Mannschreck, H. Zinner, N. Pustet, Chimia 43 (1989) 165.
[3] B. Stephan, H. Zinner, F. Kastner, A. Mannschreck, Chimia 10 (1990) 336.
[4] J. Veciana, M.I. Crespo, Angew. Chem., Int. Ed. Engl. 30 (1991) 74.
[5] M. Jung, V. Schurig, J. Am. Chem. Soc. 114 (1992) 529.
[6] V. Schurig, M. Jung, M. Schleimer, F.-G. Klärner, Chem. Ber. 125 (1992) 1301.
[7] M. Jung, M. Fluck, V. Schurig, Chirality 6 (1994) 510.
[8] D. Casarini, L. Lunazzi, S. Alcaro, F. Gasparrini, C. Villani, J. Org. Chem. 60 (1995) 5515.
[9] C. Wolf, W.A. König, C. Roussel, Liebigs Ann. (1995) 781.
[10] C. Wolf, D.H. Hochmuth, W.A. König, C. Roussel, Liebigs Ann. (1996) 357.
[11] D.H. Hochmuth, W.A. König, Liebigs Ann. (1996) 947.
[12] C. Wolf, W.H. Pirkle, C.J. Welch, D.H. Hochmuth, W.A. König, G.-L. Chee, J.L. Charlton, J. Org. Chem. 62 (1997) 5208.
[13] K. Cabrera, M. Jung, M. Fluck, V. Schurig, J. Chromatogr. A 731 (1996) 315.
[14] V. Schurig, F. Keller, S. Reich, M. Fluck, Tetrahedron: Asymmetry 8 (1997) 3475.
[15] F. Gasparrini, D. Misiti, M. Pierini, C. Villani, Tetrahedron: Asymmetry 8 (1997) 2069.
[16] K. Lorenz, E. Yashima, Y. Okamoto, Angew. Chem., Int. Ed. Engl. 110 (1998) 1922.
[17] J. Oxelbark, S. Allenmark, J. Org. Chem. 64 (1999) 1483.
[18] O. Trapp, V. Schurig, J. Am. Chem. Soc. 122 (2000) 1424.
[19] G. Schoetz, O. Trapp, V. Schurig, Anal. Chem. 72 (2000) 2758.

[20] O. Trapp, V. Schurig, Comput. Chem. 26 (2001) 187.
[21] S. Reich, O. Trapp, V. Schurig, J. Chromatogr. A 892 (2000) 487.
[22] L. Bachmann, E. Bechtold, E. Cremer, J. Catalysis 1 (1962) 113.
[23] E. Cremer, R. Kramer, J. Chromatogr. 107 (1975) 253.
[24] M. Reist, B. Testa, P.-A. Carrupt, M. Jung, V. Schurig, Chirality 7 (1995) 396.
[25] A.J.P. Martin, R.L.M. Synge, Biochem. J. 35 (1941) 1358.
[26] L.C. Craig, J. Biol. Chem. 155 (1944) 519.
[27] D.W. Basset, H.W. Habgood, J. Phys. Chem. 64 (1960) 769.
[28] J. Kallen, E. Heilbronner, Helv. Chim. Acta 43 (1960) 489.
[29] M. Jung, Program Simul, No. 620, Quantum Chemistry Program Exchange (QCPE), QCPE Bull. 3 (1992) 12.
[30] R.A. Keller, J.C. Giddings, J. Chromatogr. 3 (1960) 205.
[31] R. Kramer, J. Chromatogr. 107 (1975) 241.
[32] W.R. Melander, H.-J. Lin, J. Jacobson, C. Horvath, J. Phys. Chem. 88 (1984) 4527.
[33] J. Jacobson, W. Melander, G. Vaisnys, C. Horvath, J. Phys. Chem. 88 (1984) 4536.
[34] A.S. Rathore, C. Horvath, J. Chromatogr. A 787 (1997) 1.
[35] A.S. Rathore, C. Horvath, Electrophoresis 18 (1997) 2935.
[36] M. Lebl, V. Gut, J. Chromatogr. 260 (1983) 478.
[37] M. Moriyasu, K. Kawanishi, A. Kato, Y. Hashimoto, M. Sugiura, T. Sai, Bull. Chem. Soc. Jpn. 58 (1985) 3351.
[38] A. Mannschreck, L. Kießl, Chromatographia 28 (1989) 263.
[39] R. Thede, D. Haberland, E. Below, J. Chromatogr. A 728 (1996) 401.
[40] R. Thede, E. Below, D. Haberland, S.H. Langer, Chromatographia 45 (1997) 149.
[41] N.A. Katsanos, R. Thede, F. Roubani-Kalantzopoulou, J. Chromatogr. A 795 (1998) 133.
[42] R. Thede, D. Haberland, C. Fischer, J. Liq. Chromatogr. Rel. Technol. 21 (1998) 2089.
[43] J. Krupcik, P. Oswald, I. Spanik, P. Majek, M. Bajdichova, P. Sandra, D.W. Armstrong, in: P. Sandra, A.J. Rackstraw (Eds.), Proceedings of the 23rd International Symposium on Capillary Chromatography, I.O.P.M.S. vzw, Kortrijk, 2000, p. A.20.